*Article*

# Effect of Tungsten on Creep Behavior of 9%Cr–3%Co Martensitic Steels

**Alexandra Fedoseeva, Nadezhda Dudova, Rustam Kaibyshev and Andrey Belyakov *** 

Laboratory of Mechanical Properties of Nanostructured Materials and Superalloys, Belgorod National Research University, Pobeda 85, Belgorod 308015, Russia; fedoseeva@bsu.edu.ru (A.F.); dudova@bsu.edu.ru (N.D.); rustam_kaibyshev@bsu.edu.ru (R.K.)

\* Correspondence: belyakov@bsu.edu.ru; Tel.: +7-4722-58-54-57

**Abstract:** The effect of increasing tungsten content from 2 to 3 wt % on the creep rupture strength of a 3 wt % Co-modified P92-type steel was studied. Creep tests were carried out at a temperature of 650 °C under applied stresses ranging from 100 to 220 MPa with a step of 20 MPa. It was found that an increase in W content from 2 to 3 wt % resulted in a +15% and +14% increase in the creep rupture strength in the short-term region (up to $10^3$ h) and long-term one (up to $10^4$ h), respectively. On the other hand, in the long-term creep region, the effect of W on creep strength diminished with increasing rupture time, up to complete disappearance at $10^5$ h, because of depletion of excess W from the solid solution in the form of precipitation of the Laves phase particles. An increase in W content led to the increased amount of Laves phase and rapid coarsening of these particles under long-term creep. The contribution of W to the enhancement of creep resistance has short-term character.

**Keywords:** martensitic steels; creep; precipitation; electron microscopy

## 1. Introduction

The heat resistant steels with 9–12%Cr are widely used as structural materials for boilers, main steam pipes, and turbines of fossil power plants with increased thermal efficiency [1,2]. The excellent creep resistance of these steels is attributed to the tempered martensite lath structure (TMLS) consisting of prior austenite grains (PAG), packets, blocks, and laths, and containing a high density of separate dislocations and a dispersion of secondary phase particles [1–5]. Stability of TMLS is provided by $M_{23}C_6$-type carbides and MX (where M is V and/or Nb, and X is C and/or N) carbonitrides precipitated during tempering at boundaries and within ferritic matrix, respectively, and boundary Laves phase particles precipitated during creep [1,2,4–12]. MX carbonitrides, which are highly effective in pinning of lattice dislocations, play a vital role in superior long-term creep resistance of the high chromium martensitic steels, whereas boundary $M_{23}C_6$ carbides and Laves phase particles exerting a high Zener drag force stabilize the TMLS [1,2,5,7–14]. This dispersion of secondary phase particles withstands short-term creep [4,9,15]. The Laves phase provides effective stabilization of TMLS and therefore promotes creep resistance, although their effect on the rearrangement of lattice dislocation is negligibly small [9,11,15]. However, the particles of Laves phase grow with a high rate under creep condition and, at present, these boundary precipitations are considered to be responsible for the creep ductility of the P92-type steels during long-term aging [16]. The enhanced long-term creep strength could be achieved by hindering this microstructural evolution. An effective way to achieve this goal is to slow down the diffusion-controlled processes, such as the climb of dislocations, knitting reaction between dislocation and lath boundaries, particle coarsening, etc., by such substitutional additives as Co, W, and Mo [1,9,17–19].

It was recently shown that cobalt addition significantly hinders the coarsening of $M_{23}C_6$ carbides and MX carbonitrides under creep conditions, which results in the superior creep resistance of

martensitic steels [9,13,18,20]. This positive effect of Co is attributed to hindering diffusion within ferrite [9,18]. Efficiency of W as an alloying element in hindering diffusion is much higher than that of Co. As a result, W and Mo are known as effective alloying additives to enhance creep resistance of high chromium martensitic steels [1,19]. These elements provide an effective solid solution strengthening [1]. It was shown [21] that addition of 1% W gives +35 MPa increase in the creep rupture strength at 600 °C for 1000 h. However, in contrast with cobalt, the tungsten and molybdenum have limited solubility within ferrite, and their excessive content leads to precipitation of such W- and Mo-rich particles as Laves phase $Fe_2(W,Mo)$ or $M_6C$ carbides [1,7,9–12,22,23]. This depletion does not occur in the 9%Cr steel containing no or low amount of W [7]. Depletion of solid solution by these elements highly deteriorates the creep resistance [7,10,11]. It is worth noting that, at present, the most of experimental data on the effect of W on creep behavior were obtained for cobalt-free high chromium martensitic steels. The aim of the present work is to report the effect of W addition on the creep strength and microstructure evolution during creep of two 9%Cr martensitic steels containing 3%Co and distinguished by W content.

## 2. Materials and Methods

Two Co-modified P92-type steels with 2 and 3 wt % W denoted here as the 9Cr2W and the 9Cr3Wsteels, respectively, were produced by air melting as 40 kg ingots. Chemical compositions of these steels, measured by a FOUNDRY-MASTER UVR optical emission spectrometer (Oxford Instruments, Ambingdon, UK) are presented in Table 1.

**Table 1.** Chemical composition of the steels studied (wt %).

| Steel | Fe | C | Cr | Co. | Mo | W | V | Nb | B | N | Si | Mn |
|-------|-----|------|-----|-----|------|-----|-----|------|-------|------|------|-----|
| 9Cr2W | bal. | 0.12 | 9.3 | 3.1 | 0.44 | 2.0 | 0.2 | 0.06 | 0.005 | 0.05 | 0.08 | 0.2 |
| 9Cr3W | bal. | 0.12 | 9.5 | 3.2 | 0.45 | 3.1 | 0.2 | 0.06 | 0.005 | 0.05 | 0.06 | 0.2 |

Square bars with cross-section of $13 \times 13$ mm$^2$ were cast and hot-forged in the temperature interval 1150–1050 °C after homogenization annealing at 1100 °C for 1 h by the Central Research Institute for Machine-Building Technology, Moscow, Russia. Both steels were solution-treated at 1050 °C for 30 min, cooled in air, and subsequently tempered at 750 °C for 3 h. Tensile tests were carried out on specimens having a cross section of $1.4 \times 3$ mm$^2$ and a 16 mm gauge length using an Instron 5882 Universal Testing Machine (Instron, Norwood, MA, USA) at room temperature and at 650 °C with a strain rate of $2 \times 10^{-3}$ s$^{-1}$. Flat specimens with a gauge length of 25 mm and a cross section of $7 \times 3$ mm$^2$ (for 220–140 MPa) and cylindrical specimens with a gauge length of 100 mm and a diameter of 10 mm (for 120–80 MPa) were subjected to creep tests until rupture. The creep tests were carried out in the air at 650 °C under different initial stresses ranging from 80 to 220 MPa with a step of 20 MPa. The 100,000 h creep rupture strength was estimated by extrapolation of the experimental data using the Larson–Miller equation [24]:

$$P = T(\lg\tau + 36) \times 10^{-3} \tag{1}$$

where $P$ is the parameter of Larson–Miller; $T$ is temperature, (K); $\tau$ is time to rupture, (h).

The structural characterization was carried out using a transmission electron microscope, JEOL-2100, (TEM) (JEOL Ltd., Tokyo, Japan) with an INCA energy dispersive X-ray spectroscope (EDS) (Oxford Instruments, Abingdon, UK) and scanning electron microscope, Quanta 600FEG, (SEM) (FEI, Hillsboro, OR, USA) on ruptured creep specimens in the gauge sections corresponding to uniform deformation in the middle between grip portion and fracture surface. The size distribution and mean radius of the secondary phase particles were estimated by counting of 150 to 250 particles per specimen on at least 15 arbitrarily selected typical TEM images for each data point. The error bars are given according to the standard deviation. Identification of the precipitates was done on the basis of the

combination of EDS composition measurements of the metallic elements and indexing of electron diffraction patterns by TEM. The subgrain sizes were evaluated on TEM micrographs by the linear intercept method including all clearly visible (sub)boundaries. The dislocation densities in the grain and subgrain interiors were estimated as a number of intersections of individual dislocations with upper or down foil surfaces per unit area on at least six arbitrarily selected typical TEM images for each data point [25]. The dislocation observation was carried out under multiple-beam conditions with large excitation vectors for several diffracted planes for each TEM image. The W-rich $M_6C$ carbides and Laves phase particles could be clearly distinguished from other precipitates by their bright contrast in the back scattered electron (BSE) image (Z-contrast) [26]. $M_6C$ carbides and Laves phase particles were separated from each other by EDS composition measurements by TEM and particle size distribution [27]. The volume fractions of the precipitated phases were calculated by the Thermo-Calc software (Version 5.0.4 75, Thermo-Calc software AB, Stockholm, Sweden, 2010) using the TCFE7 database for the following compositions of steels (in wt %): 0.1%C-9.4%Cr-0.5%Mo-2.0 (or 3.0)%W-3.0%Co-0.2%V-0.05%Nb-0.05%N-0.005%B and Fe-balance. The following phases were chosen independently for calculation: austenite (FCC_A1), ferrite (BCC_A2), cementite, $M_{23}C_6$ carbide, $M_7C_3$ carbide, $M_6C$ carbide, and Laves phase (Fe$_2$(W, Mo) (C14).

## 3. Results

### 3.1. Tempered Martensite Lath Structure

After tempering at 750 °C, TMLS forms in both steels. However, in the 9Cr2W steel, the additional formation of subgrains was observed (Figure 1a), whereas TMLS is dominant in the 9Cr3W steel (Figure 1b). The average sizes of PAGs were 11 and 20 μm for the 9Cr2W and 9Cr3W steels, respectively. More details about the microstructure of the steels studied after normalization at 1050 °C and tempering at 750 °C can be found elsewhere [27].
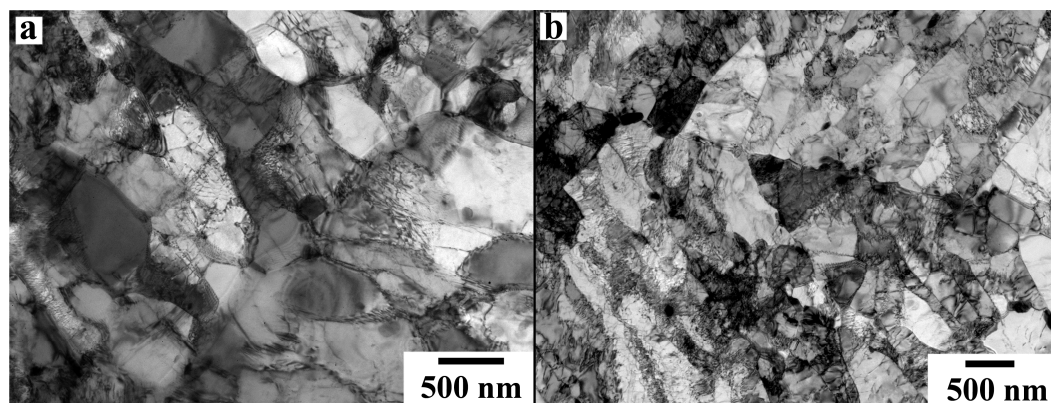


**Figure 1.** Mixed lath structure and subgrain one (**a**) in the 9Cr2W steel and homogeneous tempered martensite lath structure in the 9Cr3W steel (**b**) after normalization at 1050 °C and tempering at 750 °C.

The lath thickness was approximately 0.4 μm for both steels. The high dislocation density of approximately $2 \times 10^{14}$ m$^{-2}$ was observed within the lath and subgrain interiors. In the structure of both steels, $M_{23}C_6$ carbides located on the boundaries of PAGs, packets, blocks, and laths, and MX-type carbonitrides uniformly distributed within the martensitic laths were observed. The mean size of $M_{23}C_6$ carbides was about 90 nm. V-rich MX carbonitrides with a "wing" shape [8,15] have a mean longitudinal size of 20 nm. Nb-rich MX carbonitrides with a round shape have an average size of 40 nm. Dimensions of these particles in both steels were the same. The W-rich precipitates of $M_6C$ carbide (Fe$_3$W$_3$C) and Laves phase (Fe$_2$W) were found in the 9Cr3W steel alongside the $M_{23}C_6$ and MX particles [27]. Therefore, the solubility of (3%W + 0.5%Mo) excesses the thermodynamically equilibrium solubility limit even at the tempering temperature of 750 °C. The 1 wt %W additive provides the

precipitation of the W-rich $M_6C$ carbides and Laves phase even under tempering. No formation of thermodynamically stable W-rich Laves phases was reported in the conventional 9%Cr martensitic steels after tempering [1,2,7–12], and the appearance of the less stable W-rich $M_6C$ carbides was found only in a 10%Cr–2%W steel [23]. Under tempering, the partial transformation of $M_6C$ carbides into Laves phase particles may occur if $M_6C$ carbides are occupied by other $M_6C_6$ carbides and do not have access to W segregation in the vicinity of PAG–lath boundaries [27].

### 3.2. Tensile Test

The W effect on engineering stress-strain curves is shown in Figure 2, and yield stress (YS), ultimate tensile stress (UTS), and ductility δ are summarized in Table 2.
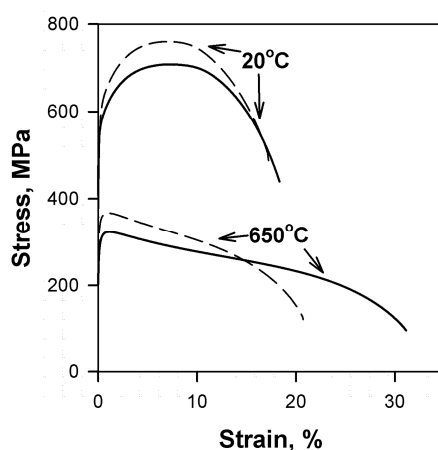


**Figure 2.** Tensile behavior of the 9Cr2W (solid lines) and 9Cr3W (dash lines) steels after heat treatment consisting of normalizing at 1050 °C and tempering at 750 °C. Tensile tests were carried out at room temperature and at 650 °C (creep test temperature).

**Table 2.** Values of yield stress (YS), ultimate tensile stress (UTS), and ductility (δ), obtained under tension, at room temperature and 650 °C for the 9Cr2W and the 9Cr3W steels.

| Steel | Temperature Test | YS, MPa | UTS, MPa | δ, % |
|---|---|---|---|---|
| 9Cr2W | 20 °C | 560 | 708 | 19 |
| | 650 °C | 295 | 325 | 32 |
| 9Cr3W | 20 °C | 570 | 760 | 18 |
| | 650 °C | 340 | 370 | 21 |

The shapes of the engineering σ−ε curves at room and elevated test temperatures for both steels were nearly the same, whereas YS and UTS are higher and δ is smaller for the 9Cr3W steel. The σ−ε curves at elevated test temperature showed the continuous yielding for both steels. After a short stage of extensive strain hardening, the apparent steady-state flow appeared and occurred up to necking. Next, post-uniform necking elongation took place up to fracture. Ductility at room test temperature was nearly the same for both steels, while at elevated temperature ductility of the 9Cr2W steel was +52% more than for 9Cr3W steel. Increments of +2% and +7% in YS and UTS at room temperature and of +15% and +14% in YS and UTS at elevated test temperature were observed for the steel with increased W content. It is obvious that these increments are provided by solid solution strengthening due to increasing W content up to 3%.

### 3.3. Creep Behavior

Figure 3a shows the creep rupture data of the steels at a temperature of 650 °C. In general, the creep rupture time of both Co-modified steels is significantly longer in comparison with the P92 steel, that is indicative of the positive effect of Co on the creep strength [1,5,15,28].
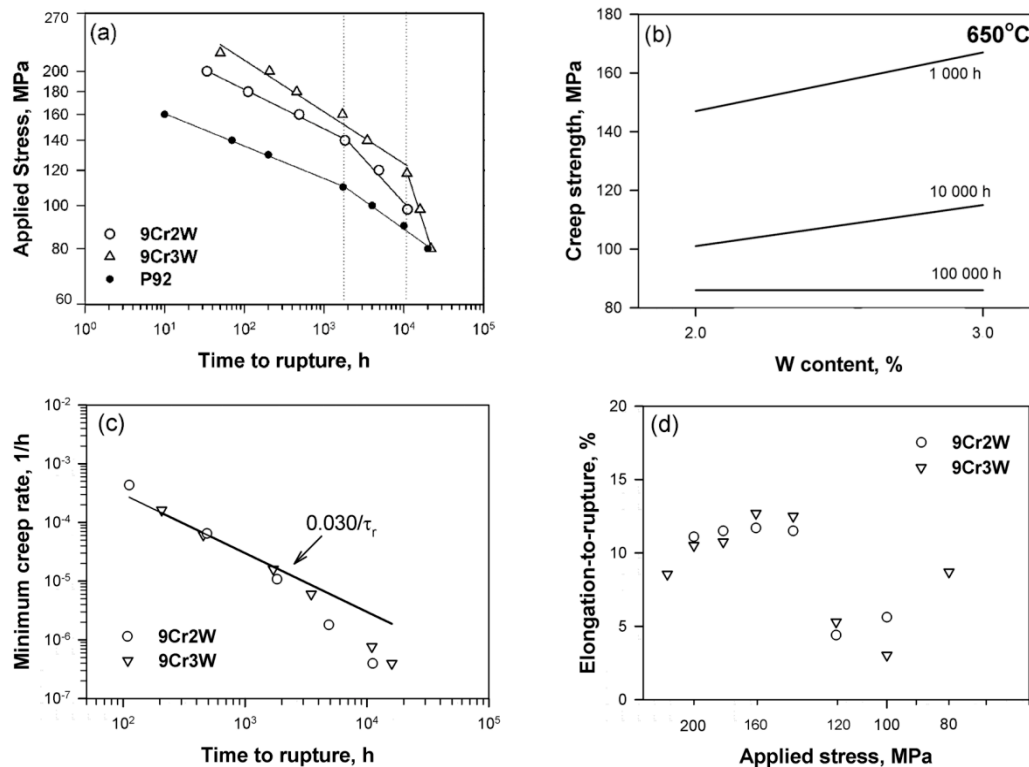


**Figure 3.** (**a**) Time to rupture vs. stress curves for the 9Cr2W and 9Cr3W steels in comparison with data for a P92 steel [2,7]; (**b**) the 1000 h, 10,000 h, and 100,000 h creep rupture strengths of steels at 650 °C as a function of W content; (**c**) minimum creep rate as a function of time to rupture for the 9Cr2W and 9Cr3W steels; and (**d**) applied stress vs. elongation-to-rupture for the 9Cr2W and 9Cr3W steels. The dotted lines in (**a**) indicate the time to rupture corresponding to the creep strength breakdown.

In the short-term region up to $10^3$ and $10^4$ h, the creep strength increase is +15% and +14% from 145 to 167 MPa and from 101 to 115 MPa, respectively, due to increased W content from 2 to 3 wt %. In the long-term creep region, the effect of W additives on the creep strength tends to diminish. For both steels the 100,000 h creep rupture strength of ~85 MPa predicted through the Larson–Miller parameter (Figure 3b) is nearly the same, and, therefore, the positive effect of W disappears. However, this value is 15% higher than the creep rupture strength of ~72 MPa for the P92 steel predicted through the Larson–Miller parameter from data published in previous works [28,29].

It was recently shown that creep strength breakdown is a tertiary creep phenomenon [7,13]. The Monkman–Grant relationship relating the rupture time, $\tau_r$, to the minimum or steady-state creep rate is described as the Equation (2):

$$\tau_r = \left( c' / \dot{\varepsilon}_{min} \right)^{m'}, \tag{2}$$

where $c'$ and $m'$ are constants. This relationship is used for the prediction of creep life of heat-resistant steels [1,13]. Analysis of Equation (2) for the studied steels (Figure 3c) shows that this approach is suitable for describing the relation of rupture time with the offset strain rate, $\dot{\varepsilon}_{min}$. For short-term conditions, which corresponds to $\tau_r$ less than approximately 2000–3500 h, $\tau_r$ is inversely proportional to $\dot{\varepsilon}_{min}$ (Figure 3c) at $m' = 1$ [13]. The constant $c'$ is $3.0 \times 10^{-2}$. For long-term conditions, which correspond to a $\tau_r$ greater than approximately 2000–3500 h, the relationship between $\tau_r$ and $\dot{\varepsilon}_{min}$

deviates downward. The transition from short-term creep to a long-term one appears as the deviation from the linear dependence described by Equation (2), which indicates $m' < 1$ [13]. Loss of ductility occurs at low stresses of 120–100 MPa in both steels (Figure 3d). For the 9Cr2W steel, a decrease in the elongation-to-rupture correlates with the creep strength breakdown appearance in Figure 3a, while for the 9Cr3W steel, the changes in elongation-to-rupture have irregular character. For high stresses from 220 to 140 MPa, elongation-to-rupture increases from 8% to 13%, then remarkably reduces to 3–5% at low stresses of 120 and 100 MPa, and then increases to 8% at 80 MPa. The relation of loss of ductility and creep strength breakdown is not revealed for the 9Cr3W steel. In contrast with the dependencies of the applied stress vs. the rupture time (Figure 3a), there was no distinct inflection point for the transition from the short-term region to the long-term one by the shapes of aforementioned curves. The minimum creep rate decreased from approximately $10^{-7}$ to $10^{-10}$ s$^{-1}$ with a decrease in the applied stress from 220 to 100 MPa. There was a linear dependence between the minimum creep rate and the applied stress (Figure 4). The experimental data obey a power law relationship throughout the whole range of the applied stress of the usual form [1,7,13]:

$$\dot{\varepsilon}_{min} = A \times \sigma^n \exp\left(\frac{-Q}{RT}\right), \tag{3}$$

where $\dot{\varepsilon}_{min}$ is the minimum creep rate, $\sigma$ is the applied stress, $Q$ is the activation energy for a plastic deformation, $R$ is the gas constant, $T$ is the absolute temperature, $A$ is a constant, and $n$ is the "apparent" stress exponent.
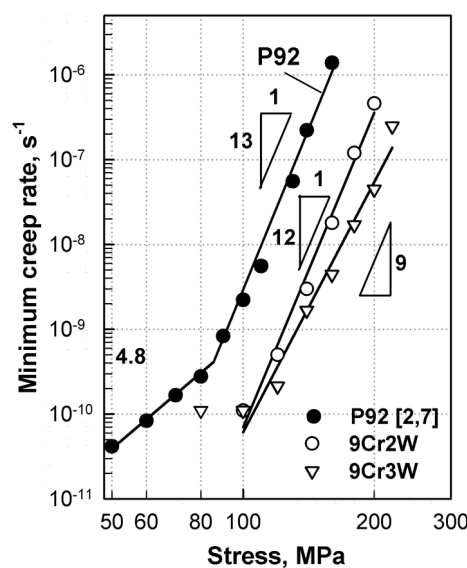


**Figure 4.** Minimum creep rate as a function of time to rupture for the 9Cr2W and 9Cr3W steels in comparison with data for the P92 steel [2,7].

For the applied stresses from 220 to 100 MPa, these plots provide the best linear fit with a regression coefficient of 0.98 for $n = 12$ and 9 for the 9Cr2W and 9Cr3W steels, respectively. This $n$ value at all tested stress regimes remains constant. The steady-state creep of the 9Cr2W and 9Cr3W steels was controlled using the same process for the short- and long-term regions at a creep rate ranging from $10^{-6}$ to $10^{-10}$ s$^{-1}$. This clearly indicates that there is no creep strength breakdown during the steady-state creep of both steels [7,13]. However, for the 9Cr3W steel, minimum creep rate at 80 MPa is similar with that at 100 MPa, which indicates the change in the process that controls the steady-state creep.

### 3.4. Crept Microstructures

SEM-BSE and TEM images of both steels after creep rupture tests are shown in Figure 5.

Laves phase, enriched by W and Mo, could be distinguished as the white particles in Z-contrast, and Cr-enriched $M_{23}C_6$ carbides as the grey particles on the grey background of matrix [10,30]. The short-term creep tests ($\leq$2000 h) did not change the lath structure in both steels (Figure 5a,b). W-rich particles exhibited nearly round shape. After the long-term creep rupture tests ($\geq$2000 h) the lath thickness increased (Figure 5c,d), and transformation of the lath structure into subgrain structure took place in both steels. The well-defined subgrain structure evolved in the 9Cr2W steel, only. TEM studies support this conclusion (Figure 5e,f). In the 9Cr2W steel, the subgrains rapidly grew from 0.6 to 1.5 μm after 2000 h (Figure 6a), whereas in the 9Cr3W steel, this size insignificantly changed from 0.6 to 0.7 μm (Figure 6b). It should be noted that upon further creep tests from 2000 to 10,000 h, the subgrain sizes remained almost unchanged in both steels (Figure 6a,b).
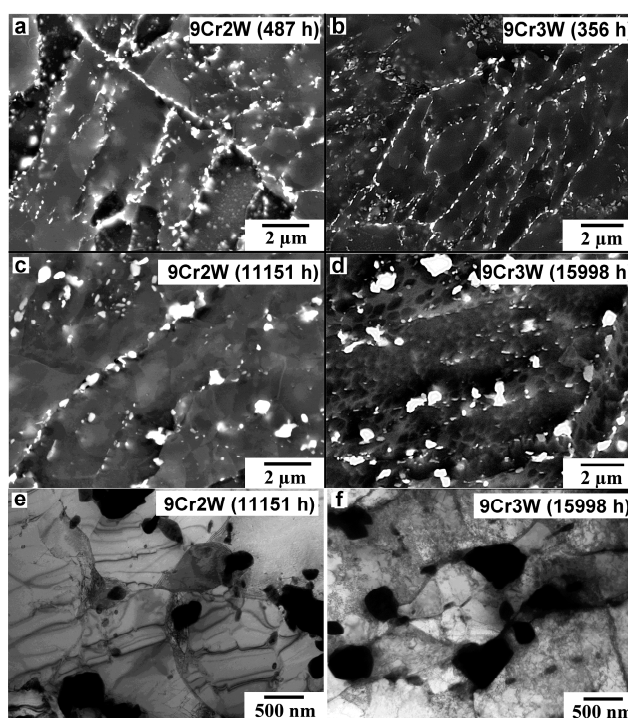


**Figure 5.** Microstructure of the 9Cr2W (**a,c,e**) and 9Cr3W (**b,d,f**) steels after creep rupture tests at 650 °C under the stress of: (**a**) 160 MPa, 487 h; (**b**) 180 MPa, 356 h; (**c,e**) 100 MPa, 11,151 h; (**d,f**) 100 MPa, 15,998 h; obtained by SEM (**a–d**) and TEM (**e,f**).

There is a difference in the effect of creep on the distributions of second phase particles in the two steels. In the 9Cr3W steel, the fine particles densely distributed along the boundaries can be seen after short-term creep (Figure 5b), whereas in the 9Cr2W steel, these precipitates were slightly coarser, and their density was less (Figure 5a).

**$M_{23}C_6$ carbides.** In the 9Cr2W steel, coarsening of $M_{23}C_6$ carbides occurred faster than in the 9Cr3W steel during creep tests (Figure 6c,d). Mean size of these carbides increased to 200–250 nm after 1000 h in the 9Cr2W steel (Figure 6c), whereas in the 9Cr3W steel, the size of these carbides remained less than 100 nm up to rupture times of ~5000 h (Figure 6d). Therefore, the W addition enhanced the coarsening resistance of $M_{23}C_6$ carbides in short-term creep conditions. At the same time, under long-term creep conditions, the average dimension of $M_{23}C_6$ carbides and their morphology became essentially the same in both steels. The average Cr and W contents in the $M_{23}C_6$ carbides were the same in both steels and tended to slightly increase with increasing rupture time (Figure 7a). In contrast, the portion of Fe decreased with increasing rupture time. Under long-term exposure, the chemical composition of $M_{23}C_6$ carbides tended to approach the thermodynamically equilibrium composition (Table 3).
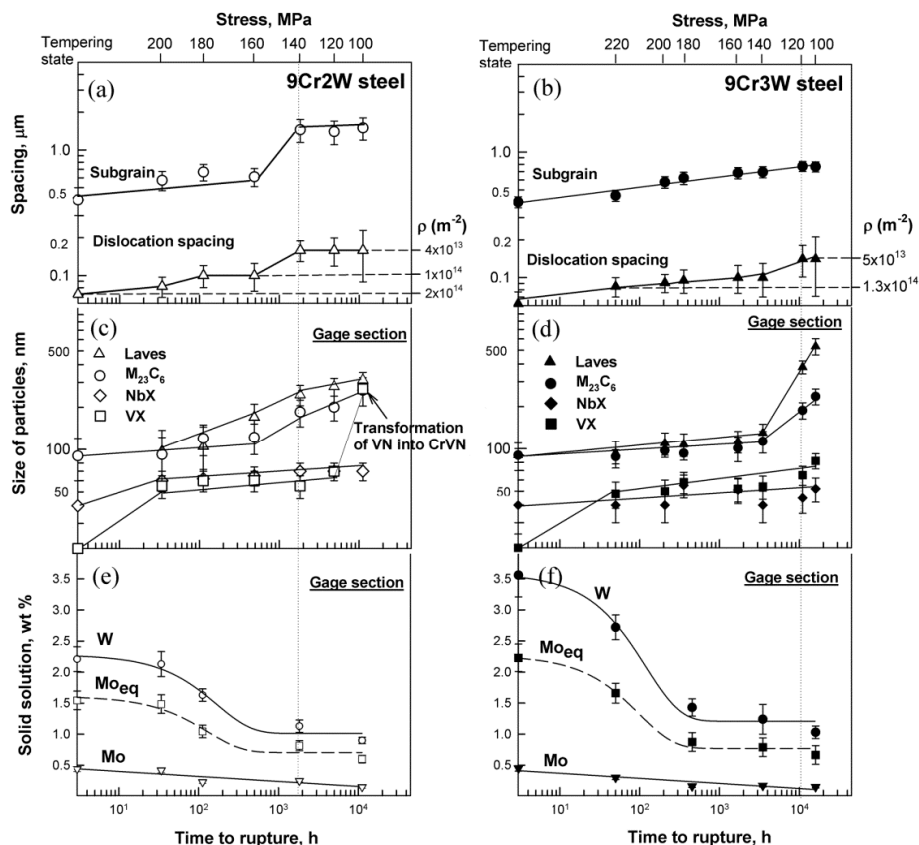
**Figure 6.** Mean size of spacing (**a**,**b**), mean size of particles of different phases (**c**,**d**), and change in W and Mo content in the solid solution (**e**,**f**) as function of time in the 9Cr2W (**a**,**c**,**e**) and 9Cr3W (**b**,**d**,**f**) steels during creep tests at 650 °C under the stresses of 100–220 MPa. The vertical dotted lines indicate the time to rupture corresponding to the creep strength breakdown. $Mo_{eq} = Mo + 0.5W$.
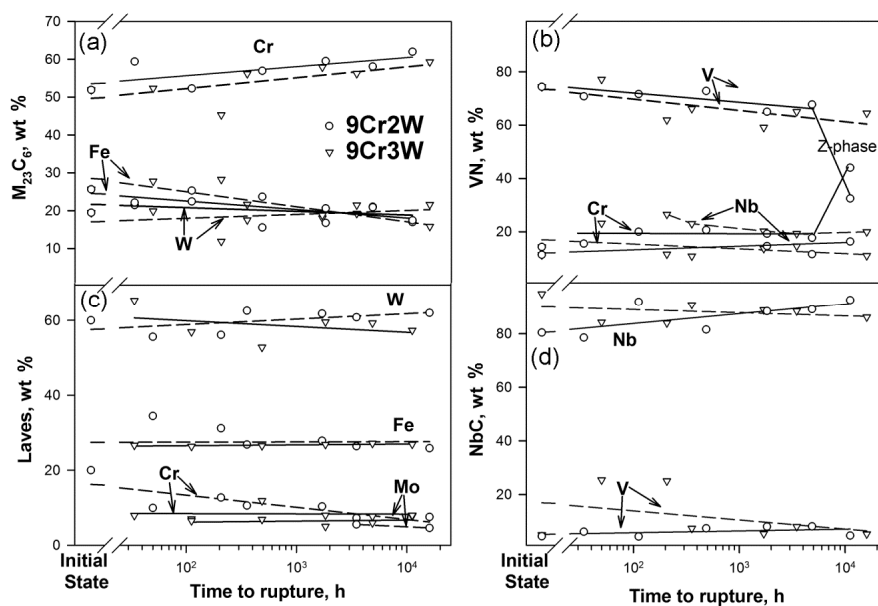


**Figure 7.** Change in the chemical compositions of (**a**) $M_{23}C_6$ carbides; (**b**) V-rich MX; (**c**) Laves phase particles; and (**d**) Nb-rich MX during creep tests at 650 °C under the stresses of 100–220 MPa.

**Table 3.** Weight fraction of elements in the different phases in the steels studied at 650 and 750 °C as calculated by Thermo-Calc.

| Element | | Cr | Fe | W | V | Nb | N | C | Mo | Co. |
|---|---|---|---|---|---|---|---|---|---|---|
| | | | | | 650 °C (Creep) | | | | | |
| MX | 9Cr2W | - | - | - | 61.98 | 17.67 | 18.25 | 0.51 | - | - |
| | 9Cr3W | - | - | - | 61.96 | 18.59 | 17.78 | 0.44 | - | - |
| M$_{23}$C$_6$ | 9Cr2W | 60.54 | 14.08 | 7.50 | 0.44 | - | - | 5.00 | 12.25 | - |
| | 9Cr3W | 60.32 | 13.95 | 8.59 | - | - | - | 5.00 | 11.24 | - |
| Laves | 9Cr2W | 6.26 | 32.57 | 56.99 | - | - | - | - | 3.99 | - |
| | 9Cr3W | 6.42 | 32.20 | 57.77 | - | - | - | - | 3.42 | - |
| Solid solution | 9Cr2W | 8.39 | 87.59 | 0.68 | 0.02 | - | - | - | 0.18 | 3.13 |
| | 9Cr3W | 8.47 | 87.16 | 0.68 | 0.04 | - | - | - | 0.16 | 3.13 |
| | | | | | 750 °C (Tempering) | | | | | |
| MX | 9Cr2W | - | - | - | 61.29 | 17.99 | 17.73 | 0.77 | - | - |
| | 9Cr3W | - | - | - | 59.50 | 19.38 | 17.78 | 0.70 | - | - |
| M$_{23}$C$_6$ | 9Cr2W | 51.78 | 20.61 | 13.92 | - | - | - | 4.83 | 8.03 | - |
| | 9Cr3W | 51.32 | 20.30 | 16.83 | | | | 4.78 | 5.80 | - |
| Laves | 9Cr2W | 5.35 | 33.62 | 56.49 | - | - | - | - | 4.31 | - |
| | 9Cr3W | 5.50 | 33.27 | 57.22 | - | - | - | - | 3.76 | - |
| Solid solution | 9Cr2W | 8.51 | 86.42 | 1.60 | 0.03 | - | - | - | 0.37 | 3.00 |
| | 9Cr3W | 8.60 | 85.98 | 1.63 | 0.04 | - | - | - | 0.32 | 3.00 |

**Laves phase.** The precipitation behavior of Laves phase in the two steels was quite different (Figure 6c,d). In the 9Cr2W steel, the precipitation of Laves phase particles started to occur with a high rate under creep condition. Next, these particles gradually grew with a high rate up to 250 nm at creep rupture time of 11,151 h (Figure 6c). In contrast, in the 9Cr3W steel, the particles of Laves phase precipitated under tempering remained their size of ~100 nm up to 5000 h of creep tests. Then, the rapid coarsening of Laves phase started to occur, and their average size attained ~550 nm at creep rupture time of ~16,000 h (Figure 6d). Thus, high W content slowed down the coarsening of Laves phase and provided the improved coarsening resistance of Laves phase up to about 10,000 h. However, upon further creep, the extensive precipitation of Laves phase induced their growth with an increased rate. The final average size of Laves phase particles in the 9Cr3W steel became even higher than that in the 9Cr2W steel (530 nm and 312 nm, respectively). In the 9Cr3W steel, the volume fraction of Laves phase was significantly higher (2.394%) in comparison with the 9Cr2W steel (1.315%) as calculated by Thermo-Calc software (Table 4). It is indicative of the full depletion of excess content of W at 650 °C from the solid solution under long-term creep.

**Table 4.** The volume fraction of second phases in the steels at 650 °C as calculated by Thermo-Calc.

| Phase | Volume Fraction (%) | |
|---|---|---|
| | 9Cr2W Steel | 9Cr3W Steel |
| M$_{23}$C$_6$ | 1.958 | 1.966 |
| MX | 0.246 | 0.238 |
| Laves phase | 1.315 | 2.394 |

In both steels, Fe and Cr contents insignificantly decreased in the Laves phase, and Mo content slightly increased during creep (Figure 7c). W content decreased in the 9Cr2W steel, whereas in the 3 wt % W steel it increased. However, these chemical composition changes of the Laves phase particles were insignificant. Therefore, the Laves phase particles initially precipitated in accordance with the thermodynamically equilibrium content (Table 3), and their coarsening was not associated with the changes in their chemical composition.

No evidence for $M_6C$ carbides presence in the 9Cr3W steel was found after creep tests. These carbides were replaced by more stable Laves phase under short-term creep as in other high-chromium martensitic steels [22].

**Nb-rich MX carbonitrides.** Thermo-Calc calculation predicted the existence of a unified (V,Nb)N nitride with a very low C content at 650 °C only in both steels (Table 4), whereas Nb-rich and V-rich separation of MX phase remained under creep condition at this temperature. In the 9Cr3W steel, Nb-rich MX carbonitrides grew from 40 to 50 nm under long-term creep condition (Figure 6d). In contrast, in the 9Cr2W steel, they rapidly grew from 40 to 60 nm under short-term creep conditions and then to 70 nm under long-term creep conditions (Figure 6c). Thus, W additives hindered the coarsening of Nb-rich MX carbonitrides. Effect of W additions is more pronounced under short-term creep. Nb and V content in the Nb-rich MX particles slightly increased and decreased, respectively, with increasing rupture time (Figure 7d) in opposition to thermodynamically equilibrium values (Table 3).

**V-rich MX carbonitrides.** The average size of V-rich MX particles attained 60 nm after long-term creep tests in both steels. In the 9Cr2W steel, the well-known replacement of V-rich MX carbonitrides by Z-phase (CrVN nitride), which is in fact the most thermodynamically stable nitride [31,32], started to occur after ~5000 h. The full transformation of all V-rich MX carbonitrides was found after 10,000 h of creep tests. The mean size of Z-phase was about 300 nm. Therefore, the size of V-rich carbonitrides increased by a factor of ~4.5 and they could not more contribute to the creep resistance of the 9Cr2W steel (Figure 6c). +1 wt %W additive shifted the onset of this transformation from 5000 h to 16,000 h; the separate Z-phase particles in the 9Cr3W steel were revealed after 16,000 h [33]. Nb content in the V-rich MX particles slightly increased with rupture time in both steel (Figure 7b). V content in the V-rich MX particles tended to decrease in the 9Cr3W steel with rupture time. At rupture time ≤5000 h, in the 9Cr2W steel, the V and Cr contents were essentially independent on the rupture time. Therefore, no gradual increase in Cr content within the V-rich MX particles resulting in transformation of their cubic lattice into tetragonal lattice of Z-phase [20,32,34] was detected.

**Solid solution.** Solid solution of the 9Cr3W steel (Figure 6f) was more enriched by W than that of the 9Cr2W steel (Figure 6e) during short-term creep up to time *t* of ~500–700 h. After this exposure, there is no significant difference in W content in the solid solution of two steels.

Depletion of W and Mo from the solid solution took place with increasing rupture time. However, the rate of the W depletion was higher in the 9Cr3W steel under short-term creep conditions. Depletion of W, $f(W)$, from the solid solution could be described as:

$$f(\text{W}) \sim 1.3 exp(-0.0059t) \quad \text{for the 9Cr2W steel,} \tag{4}$$

$$\text{and } f(\text{W}) \sim 2.4 exp(-0.0083t) \quad \text{for the 9Cr3W steel.} \tag{5}$$

Depletion of Mo, $f(Mo)$, from the solid solution could be described as:

$$f(\text{Mo}) \sim -0.08t \quad \text{for both steels.} \tag{6}$$

This finding indicates the strong dependence of W content on the rupture time up to an achievement of the thermodynamically equilibrium value of W in the ferritic matrix (Table 3). At rupture time ≥700 h, the $Mo_{eq} = \Sigma(Mo + 0.5W)$ [35] was the same for both steels since no significant difference in W and Mo content was found in the ferritic matrix of both steels by TEM.

## 4. Discussion

### 4.1. Contribution of W to the Solid Solution Strengthening

The experimental data showed that increasing W content from 2 to 3 wt % improves the creep resistance of the 0.1C-9Cr-3Co-0.5Mo-VNbBN steel at 650 °C under short-term creep conditions due to solid solution strengthening as main hardening mechanism. As a result, the TMLS essentially remains

in the 9Cr3W steel, whereas a well-defined subgrain structure evolves in the 9Cr2W steel. Despite this fact, the creep strength of the 9Cr3W steel approaches to the level of the 9Cr2W steel with increasing rupture time up to $10^5$ h according to estimation by Larson–Miller parameter. It is worth noting that effect of Co on the microstructural evolution under creep is nearly the same [18]. However, both Co and W additions could not prevent the breakdown of creep strength taking place at a rupture time of ~2000 h for the P92 steel and the 9Cr2W steel, and at a rupture time of ~10,000 for the 9Cr3W steel (Figure 3a,c).

Mo$_{eq}$ content in the solid solution of both steels is significantly higher than the solubility limit for these elements at 650 °C and the precipitation of Laves phase provides approaching of W and Mo contents to their thermodynamically equilibrium levels under creep condition. It is known [1,7,10–12,15,22] that the precipitation of Laves phase during creep is hindered by low rate of these substitutional elements diffusion. The continuous decrease in W content in the solid solution indicates the continuous decomposition of the supersaturated solid solution accompanied by the precipitation of the fine Laves phase particles during creep tests. Under long-term condition, the volume fraction of Laves phase attains the thermodynamically equilibrium value (Table 4). The same Mo$_{eq}$ value in the solid solution of both steels is attained after 700 h of short-term creep exposure. This indicates no advantage in solid solution strengthening for the 9Cr3W steel after 700 h of creep test.

However, the 9Cr3W steel demonstrates +14% increments in creep strength even after 700 h of creep testing. Increasing W content up to 3% contributes to creep strength not only by solid solution strengthening but by creation the preconditions for improved creep strength, such as homogeneous TMLS, increased dislocation density, and narrow size distributions of boundary particles after tempering, which provide advanced creep strength upon creep time more than 700 h. Therefore, under short-term creep, the W addition slows down the rearrangement of lattice dislocations by climb that may prevent the aforementioned transformation of lath boundaries to sub-boundaries. However, under long-term conditions, a saturation of the solid solution by W and Mo is the same in both steels and the retardation of dislocation climb by W addition could not provide the stabilization of TMLS. It is obvious that the influence of W content on the stability of TMLS under long-term creep conditions is attributed to its effect on a dispersion of secondary phase.

## 4.2. Contribution of W to the Particle Strengthening

The experimental data showed that increasing W content from 2 to 3 wt % improves the creep resistance of the steel in the short-term conditions due to sluggish kinetics of the coarsening of M$_{23}$C$_6$ carbides, precipitation of fine Laves phase particles, and preventing transformation of TMLS into subgrain structure. The effect of W on the coarsening behavior of M$_{23}$C$_6$ carbides and Laves phase was considered in the companion work [36] in sufficient details. In that study, we briefly summarize that 1 wt % W addition affects the size distribution of these two types of particles after tempering that leads to the difference in the coarsening behavior between two steels [36] during creep. In the work [37], it was found that the coarsening of M$_{23}$C$_6$ carbides correlates with the changes in their chemical composition. It is worth noting that the coarsening of M$_{23}$C$_6$ carbides in both steels is accompanied by an increase in Cr and W contents and a decrease in Fe content (Figure 6a). In work [37], it has been observed that M$_{23}$C$_6$ carbides grow during 50,000 h up to the chemical equilibrium. In both steels, the character of evolution of chemical composition of M$_{23}$C$_6$ carbides is essentially the same. The Cr and (W + Mo) contents in M$_{23}$C$_6$ carbides increase at the expense of Fe and reach the thermodynamically equilibrium values (Table 3). It is worth noting that Thermo-Calc calculation at 650 °C predicts the Cr and (W + Mo) content in M$_{23}$C$_6$ carbides higher and lower, respectively, than that at 750 °C. Under tempering condition, only Cr content attained thermodynamically equilibrium value in M$_{23}$C$_6$ carbides. Cr atoms diffuse slightly slower than Fe atoms in ferrite, and the diffusion rate of W and Mo atoms is the lowest in comparison with Cr [38]. This is the reason for approaching the thermodynamically equilibrium chemical composition of M$_{23}$C$_6$ carbides during a long-term exposure.

In both steels, the various second phase particles pin the lath boundaries. MX particles homogeneously distributed within the lath exert Zener drag pressure, which can be evaluated as [9,15,23,39,40]:

$$P_Z = \frac{3\gamma F_V}{d}, \tag{7}$$

where $\gamma$ is the boundary surface energy per unit area (0.153 J m$^{-2}$) [15,40], $F_v$ is the volume fraction of particles calculated by Thermo-Calc, and $d$ is a mean size of particles, m.

The boundary particles of M$_{23}$C$_6$ and Laves phases exert Zener drag pressure estimated as [9,15,23, 39,40]:

$$P_B = \frac{\gamma F_{vB} D}{d^2}, \tag{8}$$

where $D$ is subgrain size or lath width, $\mu$m, and $F_{vB}$ is the fraction of particles located at the boundaries. The pinning pressures were calculated separately for M$_{23}$C$_6$ carbides and Laves phase according with:

$$P_B = \frac{\gamma F_{vB} D_0}{d_0^2} \cdot \frac{\beta_i}{\beta_0}, \tag{9}$$

where $\beta_i$ is density of M$_{23}$C$_6$ carbides or Laves phase, located along boundaries, for each applied stress. Calculation of Zener drag pressure for the different kinds of particles was considered in the previous work [9] in details.

+1 wt % W addition as well as an applied stress affect the particles sizes and their volume fractions (Figure 6 and Table 3). As a result, there is a difference in the pinning pressure between the two steels, and Zener drag pressure depends on the creep test time (Figure 8). Both steels contain essentially the same volume fraction of MX carbonitrides, and the pinning pressure from these particles ($P_Z$) is the same for both steels. At high applied stress, MX carbonitrides give a minor contribution to the total Zener pressure due to the low volume fraction of these particles and random distribution within subgrain and laths.

In the 9Cr2W steel, the M$_{23}$C$_6$ carbides gives the main contribution to overall Zener drag force at any applied stress [23], whereas in the 9Cr3W steel the highest Zener drag is exerted by Laves phase particles at the applied stresses more than 100 MPa [39]. Only at an applied stress of 100 MPa the Zener drag exerted by M$_{23}$C$_6$ carbides in this steel (9Cr3W) becomes higher than that exerted by Laves phase particles, and the $P_B$ and $P_Z$ values originated from Laves phase and MX carbonitrides, respectively, are the same at this condition (Figure 8b). In contrast, in the 9Cr2W steel, the $P_Z$ value drops at an applied stress of 100 MPa, owing to transformation of V-rich MX carbonitrides to Z-phase, and the pinning pressures from the boundary M$_{23}$C$_6$ carbides ($P_B$) and MX carbonitrides with a random particle distribution ($P_Z$) are similar at an applied stress of 120 MPa (Figure 8a).
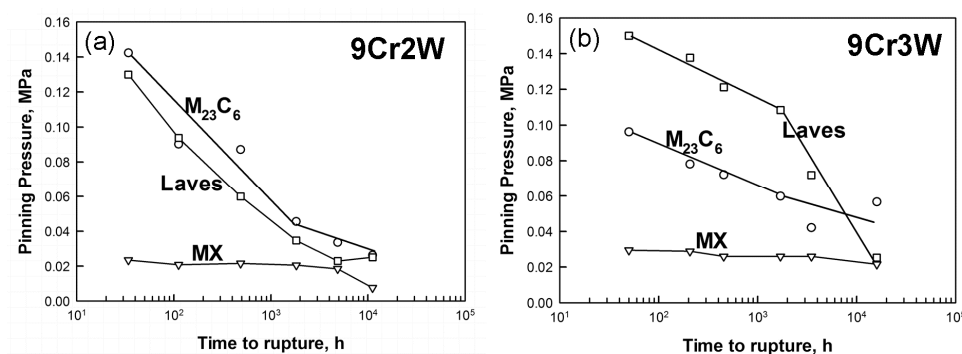


**Figure 8.** Change in the pinning pressures from different kinds of particles on the grain and lath boundaries of the (**a**) 9Cr2W steel and (**b**) 9Cr3W steel during creep tests at 650 °C under the stresses of 100–220 MPa.

Thus, the Zener pressure exerted by boundary particles remains for a long time until the particle coarsening occurs. Size stabilization of the Laves phase particles in the 9Cr3W steel provides a significant contribution to high Zener pressure, whereas their rapid coarsening removes this effect. Thus, Laves phase particles give short-term contribution to the precipitation strengthening. The decrease in Zener pressure exerted by Laves phase does not lead to the transformation of TMLS into subgrain structure as in the 9Cr2W steel because $M_{23}C_6$ carbides are able to provide the high level of Zener pressure [23] (more than 0.05 MPa) at the low stresses in the steel with 3 wt % W.

Therefore, there is no positive effect of increased W content on the creep resistance of the Co-modified P92 steel under long-term creep conditions. An alloying of 0.1C-9Cr-3Co-0.5Mo-VNbBN martensitic steel by 3%W does not seem justified for the applying at long-term creep condition (for $10^5$ h) at 650 °C. Therefore, the W content of ~2 wt % is optimal for the Co-containing high chromium martensitic steels.

## 5. Conclusions

The microstructures of two 0.1C-9Cr-3Co-0.5Mo-VNbBN martensitic steels with different content of W (2 wt % and 3 wt %) in the tempered and crept at 650 °C under stresses of 100–220 MPa conditions were studied. The main results can be summarized as follows:

1.  The structure of both steels tempered at 750 °C for 3 h is the tempered martensite lath structure with the lath thickness of 0.4 μm. An increased W content leads to the formation of W-rich Laves phase particles and $M_6C$ carbides on the boundaries in addition to the $M_{23}C_6$ carbides located also on the boundaries and MX carbonitrides distributed uniformly within the ferritic matrix.
2.  The steel with 3 wt % W content demonstrates a +15% increase in the 10,000 h creep rupture strength at 650 °C due to hindering the coarsening of the $M_{23}C_6$ carbides, MX carbonitrides and Laves phase particles. Tungsten also slows down the transformation of V-rich MX carbonitrides into Z-phase particles.
3.  An increase in W content in the steels provides an increase in the amount of Laves phase. Under long-term conditions, the depletion of excess W from the solid solution leads to the rapid coarsening of Laves phase particles; the contribution of this phase to Zener drag has a short-term character.
4.  The predicted long-term creep rupture strength for 100,000 h is about 85 MPa for both steels. This value is independent on W content due to depletion of its excess from the solid solution up to thermodynamically equilibrium value due to Laves phase precipitation. Therefore, there is no positive effect of increased W content on the creep resistance of the Co-modified P92 steel under long-term creep conditions. An alloying of 0.1C-9Cr-3Co-0.5Mo-VNbBN martensitic steel by 3%W does not seem justified for long-term creep condition (for $10^5$ h) at 650 °C. Therefore, the W content of ~2 wt % is optimal for the Co-containing high chromium martensitic steels.

**Author Contributions:** A.F., N.D., A.B. and R.K. formulated the original problem, designed the study, developed the methodology, and wrote the manuscript. A.F. and N.D. performed the experiment, collected data, and assisted with data analysis. A.B. and R.K. provided direction, guidance, and interpretation of data.

## References

1.  Abe, F.; Kern, T.U.; Viswanathan, R. *Creep Resistant Steels*; Part I; Woodhead Publishing in Materials: Cambridge, UK, 2008; p. 800.

2.  Kaybyshev, R.O.; Skorobogatykh, V.N.; Shchenkova, I.A. New martensitic steels for fossil power plant: Creep resistance. *Phys. Met. Metallogr.* **2010**, *109*, 186–200. [CrossRef]

3.  Kitahara, H.; Ueji, R.; Tsuji, N.; Minamino, Y. Crystallographic features of lath martensite in low-carbon steel. *Acta Mater.* **2006**, *54*, 1279–1288. [CrossRef]

4.  Ghassemi-Armaki, H.; Chen, R.; Maruyama, K.; Igarashi, M. Premature creep failure in strength enhanced high Cr ferritic steels caused by static recovery of tempered martensite lath structures. *Mater. Sci. Eng. A* **2010**, *527*, 6581–6588. [CrossRef]

5.  Abe, F. Analysis of creep rates of tempered martensitic 9% Cr steel based on microstructure evolution. *Mater. Sci. Eng. A* **2009**, *510*, 64–69. [CrossRef]

6.  Kostka, A.; Tak, K.-G.; Hellmig, R.J.; Estrin, Y.; Eggeler, G. On the contribution of carbides and micrograin boundaries to the creep strength of tempered martensite ferritic steels. *Acta Mater.* **2007**, *55*, 539–550. [CrossRef]

7.  Abe, F. Effect of fine precipitation and subsequent coarsening of Fe2W laves phase on the creep deformation behavior of tempered martensitic 9Cr-W steels. *Metall. Mater. Trans. A* **2005**, *36*, 321–331. [CrossRef]

8.  Taneike, M.; Sawada, K.; Abe, F. Effect of carbon concentration on precipitation behavior of $M_{23}C_6$ carbides and MX carbonitrides in martensitic 9Cr steel during heat treatment. *Metall. Mater. Trans. A* **2004**, *35*, 1255–1261. [CrossRef]

9.  Dudova, N.; Plotnikova, A.; Molodov, D.; Belyakov, A.; Kaibyshev, R. Structural changes of tempered martensitic 9%Cr-2%W-3%Co steel during creep at 650 °C. *Mater. Sci. Eng. A* **2012**, *534*, 632–639. [CrossRef]

10. Kipelova, A.; Belyakov, A.; Kaibyshev, R. Laves phase evolution in a modified P911 heat resistant steel during creep at 923K. *Mater. Sci. Eng. A* **2012**, *532*, 71–77. [CrossRef]

11. Fedorova, I.; Belyakov, A.; Kozlov, P.; Skorobogatykh, V.; Shenkova, I.; Kaibyshev, R. Laves-phase precipitates in a low-carbon 9% Cr martensitic steel during aging and creep at 923K. *Mater. Sci. Eng. A* **2014**, *615*, 153–163. [CrossRef]

12. Isik, M.I.; Kostka, A.; Yardley, V.A.; Pradeep, K.G.; Duarte, M.J.; Choi, P.P.; Raabe, D.; Eggeler, G. The nucleation of Mo-rich Laves phase particles adjacent to $M_{23}C_6$ micrograin boundary carbides in 12% Cr tempered martensite ferritic steels. *Acta Mater.* **2015**, *90*, 94–104. [CrossRef]

13. Ghassemi-Armaki, H.; Chen, R.; Maruyama, K.; Igarashi, M. Creep behavior and degradation of subgrain structures pinned by nanoscale precipitates in strength-enhanced 5 to 12 Pct Cr ferritic steels. *Metall. Mater. Trans. A* **2011**, *42*, 3084–3094. [CrossRef]

14. Yin, F.-S.; Tian, L.-Q.; Xue, B.; Jiang, X.-B.; Zhou, L. Effect of Carbon Content on Microstructure and Mechanical Properties of 9 to 12 pct Cr Ferritic/Martensitic Heat-Resistant Steels. *Metall. Mater. Trans. A* **2012**, *43*, 2203–2209. [CrossRef]

15. Dudko, V.; Belyakov, A.; Molodov, D.; Kaibyshev, R. Microstructure evolution and pinning of boundaries by precipitates in a 9 pct. Cr heat resistant steel during creep. *Metall. Mater. Trans. A* **2013**, *44*, S162–S172. [CrossRef]

16. Zhong, W.; Wang, W.; Yang, X.; Li, W.; Yan, W.; Sha, W.; Wang, W.; Shan, Y.; Yang, K. Relationship between Laves phase and the impact brittleness of P92 steel reevaluated. *Mater. Sci. Eng. A* **2015**, *639*, 252–258. [CrossRef]

17. Helis, L.; Toda, Y.; Hara, T.; Miyazaki, H.; Abe, F. Effect of cobalt on the microstructure of tempered martensitic 9Cr steel for ultra-supercritical power plants. *Mater. Sci. Eng. A* **2009**, *510*, 88–94. [CrossRef]

18. Kipelova, A.; Odnobokova, M.; Belyakov, A.; Kaibyshev, R. Effect of Co on creep behavior of a P911 steel. *Metall. Mater. Trans. A* **2013**, *44*, 577–583. [CrossRef]

19. Sawada, K.; Takeda, M.; Maruyama, K.; Ishii, R.; Yamada, M.; Nagae, Y.; Komine, R. Effect of W on recovery of lath structure during creep of high chromium martensitic steels. *Mater. Sci. Eng. A* **1999**, *267*, 19–25. [CrossRef]

20. Fedoseeva, A.; Dudova, N.; Kaibyshev, R. Creep strength breakdown and microstructure evolution in a 3%Co modified P92 steel. *Mater. Sci. Eng. A* **2016**, *654*, 1–12. [CrossRef]

21. Tsuchida, Y.; Okamoto, K. Improvement of creep rupture strength of high Cr ferritic steel by addition of W. *ISIJ Int.* **1995**, *35*, 317–323. [CrossRef]

22. Li, Q. Precipitation of Fe2W laves phase and modeling of its direct influence on the strength of a 12Cr-2W steel. *Metall. Mater. Trans. A* **2006**, *37*, 89–97. [CrossRef]

23. Dudova, N.; Kaibyshev, R. On the precipitation sequence in a 10% Cr steel under tempering. *ISIJ Int.* **2011**, *51*, 826–831. [CrossRef]

24. Wilshire, B.; Scharning, P. Prediction of long term creep data for forged 1Cr-1Mo-0.25V steel. *Mater. Sci. Technol.* **2008**, *24*, 1–9. [CrossRef]

25. Hirsch, P.B.; Howie, A.; Nicholson, R.B.; Pashley, D.W.; Whelan, M.J. *Electron Microscopy of Thin Crystals*, 2nd ed.; Krieger: New York, NY, USA, 1977; p. 563.

26. Dimmler, G.; Weinert, P.; Kozeschnik, E.; Cerjak, H. Quantification of the Laves phase in advanced 9–12% Cr steels using a standard SEM. *Mater. Charact.* **2003**, *51*, 341–352. [CrossRef]

27. Fedoseeva, A.; Dudova, N.; Glatzel, U.; Kaibyshev, R. Effect of W on tempering behaviour of a 3% Co modified P92 steel. *J. Mater. Sci.* **2016**, *51*, 9424–9439. [CrossRef]

28. Kimura, K.; Toda, Y.; Kushima, H.; Sawada, K. Creep strength of high chromium steel with ferrite matrix. *Int. J. Press. Vessels Pip.* **2010**, *87*, 282–288. [CrossRef]

29. Yoshizawa, M.; Igarashi, M.; Moriguchi, K.; Iseda, A.; GhassemiArmaki, H.; Maruyama, K. Effect of precipitates on long-term creep deformation properties of P92 and P122 type advanced ferritic steels for USC power plants. *Mater. Sci. Eng. A* **2009**, *510*, 162–168. [CrossRef]

30. Hattestrand, A.; Andren, H.O. Evaluation of particle size distributions of precipitates in a 9% chromium steel using energy filtered transmission electron microscopy. *Micron* **2001**, *32*, 489–498. [CrossRef]

31. Cipolla, L.; Danielsen, H.K.; Venditti, D.; Di Nunzio, P.E.; Hald, J.; Somers, M.A.J. Conversion of MX nitrides to Z-phase in a martensitic 12% Cr steel. *Acta Mater.* **2010**, *58*, 669–679. [CrossRef]

32. Danielsen, H.K.; Di Nunzio, P.E.; Hald, J. Kinetics of Z-Phase Precipitation in 9 to 12 pct Cr Steels. *Metall. Mater. Trans. A* **2013**, *44*, 2445–2452. [CrossRef]

33. Fedoseeva, A.; Dudova, N.; Kaibyshev, R. Effect of Tungsten on a Dispersion of M(C,N) Carbonitrides in 9% Cr Steels Under Creep Conditions. *Trans. Indian Inst. Met.* **2016**, *69*, 211–215. [CrossRef]

34. Kaibyshev, R.O.; Skorobogatykh, V.N.; Shchenkova, I.A. Formation of the Z-phase and prospects of martensitic steels with 11% Cr for operation above 590 °C. *Met. Sci. Heat Treat.* **2010**, *52*, 90–99. [CrossRef]

35. Klueh, R.L. Elevated temperature ferritic and martensitic steels and their application to future nuclear reactors. *Int. Mater. Rev.* **2005**, *50*, 287–310. [CrossRef]

36. Fedoseeva, A.; Dudova, N.; Kaibyshev, R. Effect of stresses on the structural changes in high-chromium steel upon creep. *Phys. Met. Metall.* **2017**, *118*, 591–600. [CrossRef]

37. Ghassemi-Armaki, H.; Chen, R.; Kano, S.; Maruyama, K.; Hasegawa, Y.; Igarashi, M. Strain-induced coarsening of nanoscale precipitates in strength enhanced high Cr ferritic steels. *Mater. Sci. Eng. A* **2012**, *532*, 373–380. [CrossRef]

38. Mehrer, H.; Stolica, N.; Stolwijk, N.A. Landolt Bornstein- Numerical Data and Functional Relationships in Science and Technology, New Series, Group III: Crystals and Solid State Physics. In *Diffusion in Solid Metals and Alloys*; Springer: Berlin/Heidelberg, Germany, 1990; Volume 26, pp. 47–48. ISBN 978-3-540-50886-1.

39. Fedoseeva, A.; Dudova, N.; Kaibyshev, R. Creep behavior and microstructure of a 9Cr-3Co-3W martensitic steel. *J. Mater. Sci.* **2017**, *52*, 2974–2988. [CrossRef]

40. Humphreys, F.J.; Hatherly, M. *Recrystallization and Related Annealing Phenomena*, 2nd ed.; Elsevier: Atlanta, GA, USA, 2004; pp. 91–112.